Check for updates

# Hydrogen production *via* electrolysis and ultrasound-assisted sonoelectrolysis: evaluating NiO, CoO, and MnO$_2$ catalyst performance and process efficiency

Yew Heng Teoh,*[a] Wong Yang Han,[a] Heoy Geok How,[b] Haseeb Yaqoob, [ID] *[c] Mohamad Yusof Idroas,[a] Saad Uddin Mahmud, [ID] [a] Thanh Danh Le,[d] Muhammad Ahmad[c] and Muhammad Wakil Shahzad*[c]

This study investigates the optimization of hydrogen production by comparing standard electrolysis with ultrasound-assisted sonoelectrolysis. The catalytic performance of NiO, CoO, and MnO$_2$ was evaluated at operating temperatures of 30 °C, 45 °C, and 60 °C to determine the most effective conditions for maximising H$_2$ production rate and energy efficiency. Using a design of experiments (DOE) framework and response surface methodology (RSM), predictive models were developed and experimentally validated. Sonoelectrolysis achieved a higher production rate (67.2 cm$^3$ h$^{-1}$) than standard electrolysis (62 cm$^3$ h$^{-1}$) but with reduced energy efficiency (2.14% *vs.* 4.37%) due to additional ultrasonic energy demands. For both methods, optimal conditions were consistently found at 60 °C with NiO as the catalyst. Statistical analysis showed that standard electrolysis followed a simple linear model, while sonoelectrolysis required a more complex quadratic model to capture the significant effects of temperature and catalyst type. The regression models were validated with low error rates (0.23–1.10%), providing a quantitative understanding of the performance gains and efficiency trade-offs in sonoelectrolysis, and offering guidance for advancing green hydrogen technologies.

## 1. Introduction

The over-reliance on non-renewable energy sources significantly contributes to climate change and related environmental issues.[1,2] These impacts stem from greenhouse gas (GHG) emissions during extraction, processing, and combustion, as well as from land degradation and water pollution. Global energy-related CO$_2$ emissions, as shown in Fig. 1, have trended upward steadily from 1990 to 2024.[3] These emissions trap heat in the atmosphere, contributing to global warming and causing climate instability.[4]

Tackling these challenges calls for cleaner energy choices that balance environmental, economic, and technological needs. Hydrogen is gaining attention for its ability to cut emissions in industry, transport, and power generation. It is abundant, has high energy density, and works well with variable renewables like solar and wind. "Green hydrogen," made from water electrolysis using renewable energy, is a zero-emission fuel.[5,6] Hydrogen has many benefits over rival energy sources such as ammonia and methanol. But they produce CO$_2$ or have lower energy density than hydrogen.[7-9] However, green hydrogen produced from water electrolysis releases only oxygen as a byproduct, making it a promising alternative for reducing GHG emissions.[10]

The potential of H$_2$ energy is receiving increased attention from policymakers worldwide, resulting in significant investments in hydrogen technologies and pilot projects.[11] Research into hydrogen production from renewable sources, including solar-driven water splitting and bio-based methods, is accelerating.[12] In addition to other methods, ultrasound-driven hydrogen production is emerging as a prime candidate due to its novel approaches and potential for better yields.[13]

The transmission of ultrasonic waves in a liquid medium produces two primary phenomena: acoustic streaming and acoustic cavitation.[14] Acoustic cavitation is when ultrasonic waves create microbubbles in a liquid. These bubbles rapidly grow and collapse, generating localized high-temperature and high-pressure conditions, with "hot spots" reaching about

[a] *School of Mechanical Engineering, Tuanku Syed Sirajuddin Engineering Campus, Universiti Sains Malaysia, 14300Nibong Tebal, Pulau Pinang, Malaysia*

[b] *Department of Engineering, UOW Malaysia KDU Penang University College, Batu Kawan Campus, PMT755, Persiaran Cassia Barat 3, Bandar Cassia, 14110, Simpang Ampat, Malaysia*

[c] *Mechanical & Construction Engineering Department, Northumbria University, Newcastle Upon Tyne, NE1 8ST, UK.*
*E-mail: muhammad.w.shahzad@northumbria.ac.uk*

[d] *College of Technology and Design, University of Economics Ho Chi Minh City (UEH), 59C Nguyen Dinh Chieu Street, Xuan Hoa Ward, Ho Chi Minh City, 700000, Vietnam*
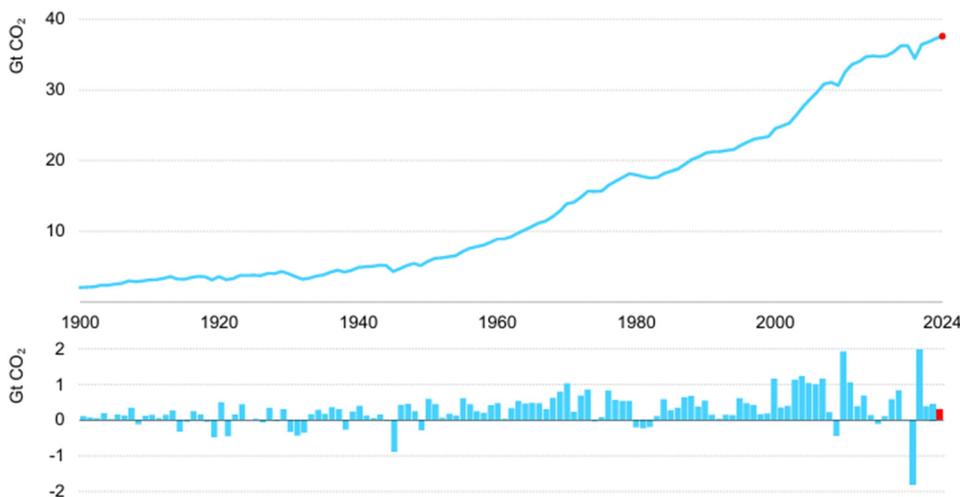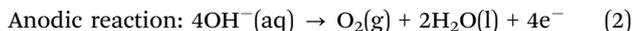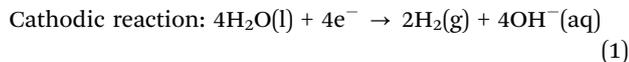
**Global energy related CO$_2$ emissions and their annual change, 1990-2024**



**Fig. 1** Global CO$_2$ emissions related to energy and their annual changes from 1990–2024.[3]

$5200 \pm 200$ K and $250 \pm$ MPa.[15] This process generates hydrogen and hydroxyl radicals from the original water molecules, which can recombine into H$_2$ and O$_2$. The reaction at the cathode and anode is shown in eqn (i) and (ii).[16]

$$\text{Cathodic reaction: } 4H_2O(l) + 4e^- \rightarrow 2H_2(g) + 4OH^-(aq) \tag{1}$$

$$\text{Anodic reaction: } 4OH^-(aq) \rightarrow O_2(g) + 2H_2O(l) + 4e^- \tag{2}$$

Numerous factors impacting H$_2$ production include bubble temperatures, acoustic power, ultrasound frequency, acoustic intensity, ambient bubble radius, dissolved gas and bulk liquid temperature.[17] Rosa et al.[18] studied the use of visible-light-driven Fe–TiO$_2$ photocatalysis combined with ultrasound and hydrogen peroxide for dye wastewater degradation, finding that while photocatalysis and ultrasound alone showed no notable change, H$_2$O$_2$ significantly enhanced hydroxyl radical generation, achieving complete Rhodamine B removal in two hours. In another research study, Chen et al.[19] reported an Ag- and Ru-modified NiFe LDH electrocatalyst for alkaline seawater electrolysis, showing low OER overpotentials at industrial current densities and excellent long-term stability ($>1000$ h), attributed to synergistic electronic regulation and improved chloride corrosion resistance. Meanwhile, Ibrahim et al.[20] developed CeO$_2$- and La$_2$O$_3$-promoted Fe/Al$_2$O$_3$ catalysts for methane decomposition to hydrogen. Utilizing ultrasonication during catalyst preparation improved metal dispersion and achieved a 93% methane conversion and 84% hydrogen yield at 800 °C. Extending ultrasound's role, Su et al.[21] examined its effect on hydrogen bubble evolution in proton exchange membrane electrolysis, revealing that it reduced bubble size and improved mass transport, enhancing kinetics without thermal side effects. On the other hand, Wei et al.[22] advanced this by preparing PdCo bimetallic nanoparticles on beta zeolite through ultrasonic-assisted galvanic replacement, resulting in excellent catalytic activity for dodecahydro-N-ethylcarbazole dehydrogenation. On the other hand, Kim et al.[23] used ultrasound-assisted electrodeposition to create CoP nanocomposites as bifunctional electrocatalysts, achieving low overpotentials and high stability for hydrogen evolution and methanol oxidation. Lastly, Wong et al.[24] explored ultrasound-driven seawater splitting with TiO$_2$, achieving high hydrogen production efficiencies by optimizing salt-scavenging effects in saline environments (Fig. 2).

Although previous studies have demonstrated the potential of ultrasound-assisted processes for enhancing hydrogen production, several limitations remain that restrict their practical application and motivated the present work. Many reported systems suffer from low overall energy efficiency due to the additional power demands of ultrasonic equipment, and optimisation efforts have rarely balanced production gains with energy costs. Experimental investigations are often constrained to specific catalysts, operating conditions, or ultrasonic parameters, leaving gaps in understanding the broader interplay between temperature, catalyst type, and acoustic field characteristics. Furthermore, limited comparative analyses between standard electrolysis and sonoelectrolysis under controlled but varied conditions make it difficult to quantify the actual benefits and trade-offs of ultrasound integration. These gaps inspired the present study.

Efficient catalysts are vital for improving hydrogen production in water splitting, addressing the challenge of the slow hydrogen evolution reaction (HER) and oxygen evolution reaction (OER), which need high overpotentials. Catalysts reduce these overpotentials, enhancing hydrogen and oxygen production. Key performance aspects to consider for catalysts include activity, stability, and efficiency.[25–27] Metals like ruthenium (Ru) are excellent due to their unique electronic properties, while platinum (Pt) based materials and IrO$_2$/RuO$_2$ are still effective and relatively low-cost options for the HER and OER.[28,29]

Using ultrasound alone for hydrogen production has limitations, as over 50% of energy can be lost as heat. Sonocatalysis improves this by adding a catalyst, enhancing bubble formation and reactive radical production, with optimal results achieved using 0.5 to
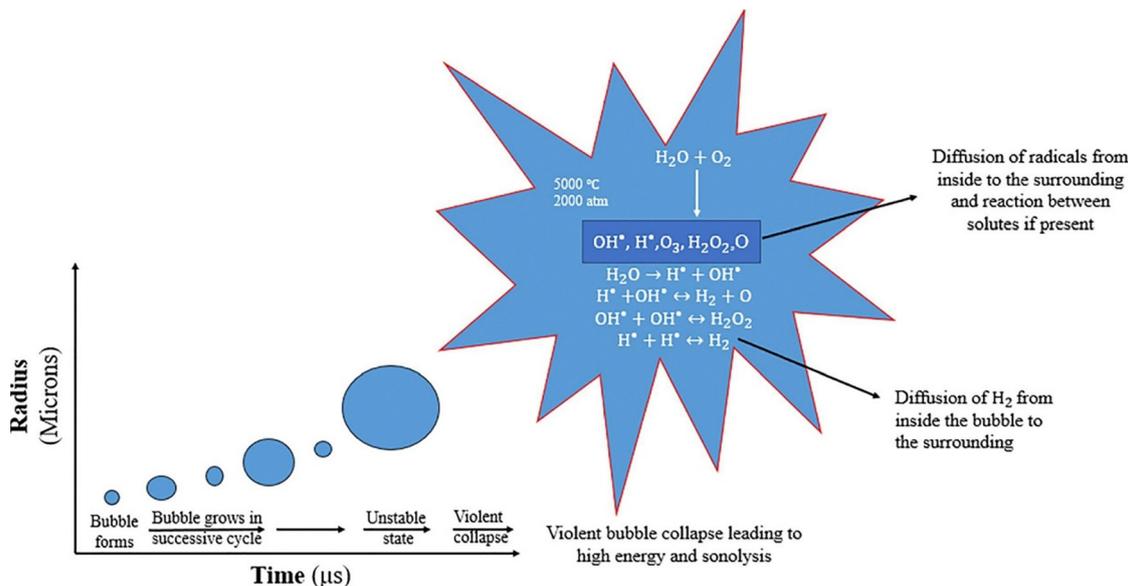
Fig. 2 The cavitation bubble grows during ultrasonication, leading to the production of sonolysis species from acoustic cavitation.[16]

1 gram of catalyst per liter. Additionally, sonoelectrocatalysis combines ultrasound and electrocatalysis, allowing ultrasound to remove gas bubbles from electrodes, improving catalyst efficiency.[30–32] It enhances mass transfer, prevents gas bubble buildup, and generates beneficial radicals like hydroxyl radicals when a catalyst is added.[33]

This study combines simulations and experiments to provide a clearer understanding of ultrasound-assisted hydrogen production. A CFD model in ANSYS is utilised to investigate the acoustic effects, while a single-cell electrolysis setup is used to test hydrogen output and efficiency both with and without ultrasound. By comparing nickel oxide (NiO), cobalt oxide (CoO), and manganese dioxide ($MnO_2$) at various temperatures through a DOE framework, and analyzing the results with RSM, the research identifies optimal conditions and demonstrates how ultrasound introduces nonlinear behavior in the process.

Unlike some earlier works in which the authors also used sonoelectrolysis but focused on different catalyst types and concentration effects under fixed operating conditions, the present study addresses a different and previously unexplored optimization dimension by treating operating temperature as a primary variable. This enables a direct examination of thermal–acoustic–electrochemical coupling effects in sonoelectrolysis. In addition, the inclusion of numerical analysis provides a physics-based interpretation of pressure-field distributions within the sonoreactor, moving beyond purely empirical observations. This integrated experimental–numerical approach offers new insights into the trade-offs between production gains and energy costs, advancing the practical development of sonoelectrocatalysis for green hydrogen.

## 2. Methodology

### 2.1 Simulation model

A CFD model is developed to improve the sonoreactor system's performance using ANSYS Mechanical's Harmonic Acoustics

module. This simulation examines sound wave behaviour and pressure changes in a cylindrical sonoreactor (135 mm internal diameter, 170 mm height) filled with water at 25 °C. An ultrasound transducer probe, inserted vertically with a 20 mm gap from the top, operates at 20 kHz and 36 W power, with a pressure amplitude of 585.9 kPa. The material is set to "Water Liquid" from the ANSYS library, with boundary conditions defined as Sound Hard for rigid surfaces, Sound Soft for open boundaries, and Pressure for the transducer tip (Fig. 3).

After completing the geometry, material properties, and boundary settings, the model undergoes harmonic acoustic analysis to predict steady-state pressure fields at ultrasound frequencies from 20 kHz to 90 kHz. The results highlight the highest and lowest acoustic pressure values in the sonoreactor for each tested frequency.

### 2.2 Design of experiment (DOE)

This research used Design-Expert 13.0 to examine the impact of different catalysts on electrolysis and sonoelectrolysis. The selected catalysts (NiO, CoO, and $MnO_2$) were chosen based on previous studies highlighting their effectiveness in improving sonoelectrolysis performance.[34–36] The catalyst concentration was uniformly set at 1.0 g $L^{-1}$, as it wasn't the main focus of the research. Two sets of DOEs were created, one for conventional electrolysis and one for sonoelectrolysis, each consisting of 17 experimental runs, totalling 34 runs, shown in Table 1. This experimental plan examined the effects of catalyst and operating temperature on $H_2$ production and energy efficiency.

Based on the DOE–RSM analysis, explicit regression equations were developed to describe the relationship between operating temperature ($A$) and catalyst type ($B$) on hydrogen production rate and energy efficiency. For electrocatalysis, eqn (i) uses a two-factor interaction (2FI) model, while sonoelectrocatalysis requires a quadratic model due to the nonlinear influence of ultrasound which is shown in eqn (ii).
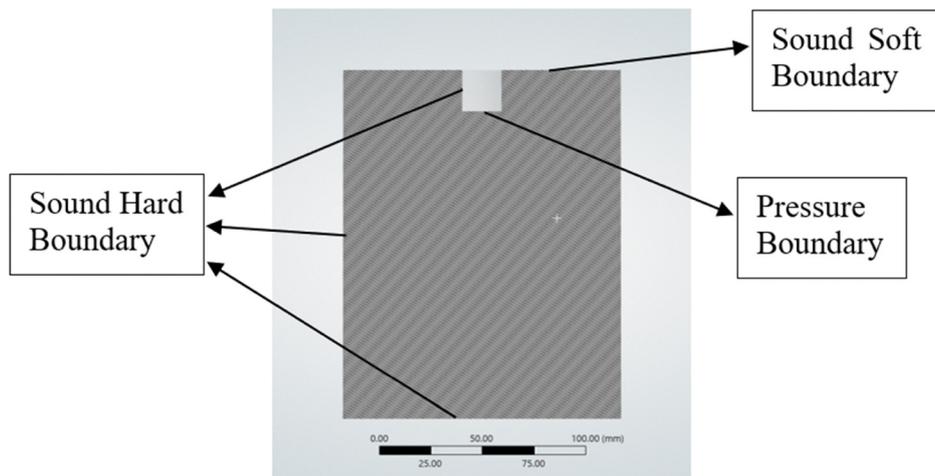
Fig. 3 Boundaries applied to the model.

Table 1 Design of experiment generated in Design-Expert 13

| | Operating temperature (°C) | Types of catalyst |
|---|---|---|
| 1 | 60 | NiO |
| 2 | 45 | NiO |
| 3 | 45 | CoO |
| 4 | 45 | CoO |
| 5 | 30 | $MnO_2$ |
| 6 | 30 | $MnO_2$ |
| 7 | 60 | CoO |
| 8 | 30 | NiO |
| 9 | 45 | $MnO_2$ |
| 10 | 30 | NiO |
| 11 | 30 | CoO |
| 12 | 45 | $MnO_2$ |
| 13 | 30 | $MnO_2$ |
| 14 | 60 | CoO |
| 15 | 45 | NiO |
| 16 | 60 | $MnO_2$ |
| 17 | 30 | $MnO_2$ |

Electrocatalysis (2FI model)[37]:

$$Y = \beta_0 + \beta_1 A + \beta_{B_1}B_1 + \beta_{B_2}B_2 + \beta_{A,B_1}AB_1 + \beta_{A,B_2}AB_2 \quad \text{(i)}$$

Sonoelectrocatalysis (quadratic model)[38]:

$$Y = \beta_0 + \beta_1 A + \beta_{B_1}B_1 + \beta_{B_2}B_2 + \beta_{A,B_1}AB_1 + \beta_{A,B_2}AB_2 + \beta_{11}A^2 \quad \text{(ii)}$$

where $Y$ represents the predicted response (hydrogen production rate or energy efficiency), $A$ is the coded temperature term, and $B_1$ and $B_2$ are indicator variables for catalyst type (with the third level as the reference). Positive coefficients indicate synergistic effects, whereas negative coefficients indicate antagonistic effects.

### 2.3 Materials and apparatus

The experiment used a water electrolysis setup comprising an electrolytic cell with two carbon electrodes (anode and cathode), a power supply, and a gas collection cylinder. Each electrode had a diameter of 5 mm and an immersed active length of 50 mm. Hydrogen evolution occurred at the cathode, and all electrochemical parameters were evaluated based on the cathode's geometric surface area, which was calculated as 7.85 cm$^2$. A 500 mL beaker contained 200 mL of distilled water mixed with NaHCO$_3$, prepared using a weighing scale and spatula, and stirred for uniformity. For sonoelectrolysis, the setup was placed in a Branson 3800 MH ultrasonic bath (40 kHz, 5.7 L capacity, heating up to 69 °C, 60 min timer) to generate ultrasonic waves while maintaining the same electrolysis configuration. NiO, CoO, and MnO$_2$ catalysts were prepared to study their effects on H$_2$ production and energy efficiency in electrolysis and sonoelectrolysis at temperatures of 30 °C, 45 °C, and 60 (Fig. 4).

The electrolysis setup was placed in the ultrasonic bath to control the temperature of the electrolyte using a water bath. As shown in Fig. 5, the electrolytic cell was immersed in distilled water to prevent corrosion of the alligator clips connected to the anode and cathode, as distilled water is an electrical insulator. It also facilitated heat transfer from the walls to the electrolyte. An inverted measuring cylinder was placed above the cathode to collect and measure the hydrogen gas produced, with the volume of displaced water indicating the gas volume generated during electrolysis.

### 2.4 Experiment procedure

A 500 ml beaker was filled with 200 ml of distilled water, and 2.5 grams of NaHCO$_3$ were added as the electrolyte. The baking soda was measured on a digital scale and mixed well with a stirrer. A customised electrolytic cell featuring two carbon electrodes was assembled and connected to a power supply using alligator clips. The electrolyte solution was poured into the cell, and a 10 ml measuring cylinder was inverted at the cathode to collect hydrogen gas. The cell was placed in the ultrasonic bath filled with distilled water, which was heated to a preset temperature. The electrolyte temperature was measured with a thermometer before starting the electrolysis process, which was carefully observed for hydrogen production rate and energy efficiency (Fig. 6).

The sonoelectrolysis process improves standard electrolysis by using ultrasonic waves to enhance reactions. The setup
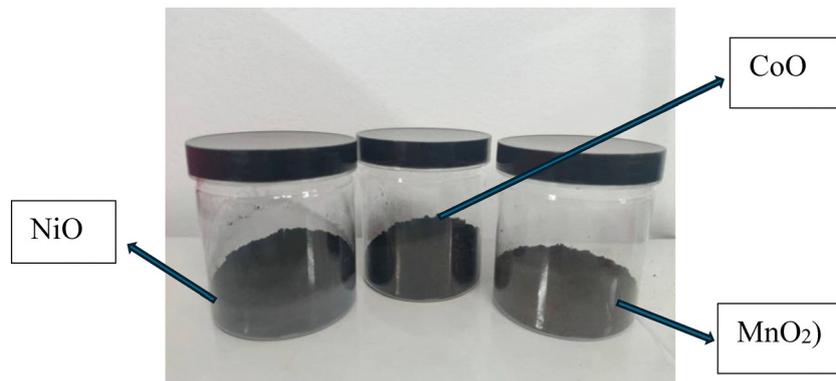
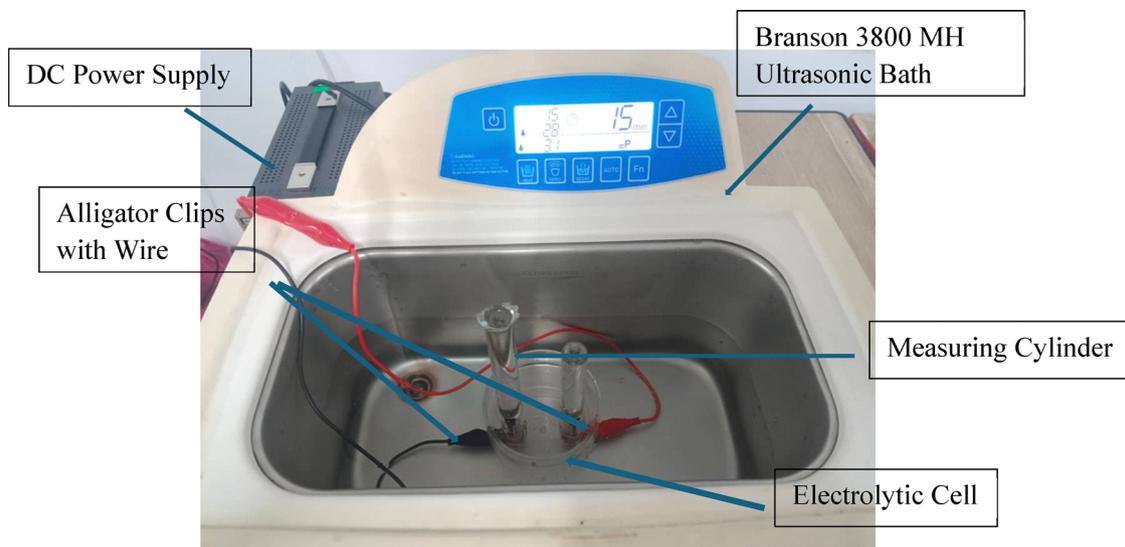Fig. 4 Types of catalyst used (NiO, CoO and MnO$_2$).



Fig. 5 Experimental setup inside the tank of the Branson 3800 MH ultrasonic bath device.

involved 200 mL of distilled water and sodium bicarbonate as the electrolyte in an electrolytic cell with carbon electrodes connected to a power supply. Ultrasonic waves were supplied by a Branson 3800 MH bath operating at 40 kHz. NiO, CoO, and MnO$_2$ nanoparticles were added to the electrolyte at a concentration of 1.0 g L$^{-1}$, ensuring uniform mixing for reliable results. The solution underwent a pre-sonication for 5 minutes to disperse the catalysts evenly, enhancing their activity during the electrochemical reactions. During sonoelectrolysis, the electrolyte temperature was continuously monitored, and the short experimental duration kept ultrasound-induced heating within a narrow range. Sonoelectrocatalysis experiments were repeated three times to obtain consistent results on gas production and energy efficiency, allowing for performance assessment of each catalyst under different conditions.

## 3. Results and discussion

This section presents simulation results on the impact of different ultrasonic frequencies on pressure distribution within the sonoreactor model. It includes an analysis of hydrogen production rates and energy efficiency from both electrocatalysis and sonoelectrocatalysis experiments, planned using the DOE method. A total of 17 runs were conducted for each method, adhering to standard procedures. Hydrogen gas production was measured using a cylinder scale, with each run repeated three times for increased reliability. The findings evaluate the performance of various catalysts at different operating temperatures to identify the most effective and energy-efficient combinations.

### 3.1 Effect of ultrasonic frequency

At low frequencies (20 kHz to 40 kHz), the pressure zones are large but not low enough to generate a significant number of bubbles, leading to powerful but infrequent collapses that don't trigger optimal chemical reactions. At higher frequencies (70 kHz to 90 kHz), many tiny bubbles form quickly but collapse weakly due to their small size, resulting in insufficient energy release.

In contrast, at mid-range frequencies like 50 kHz, there's a balance that allows for a large number of bubbles to grow
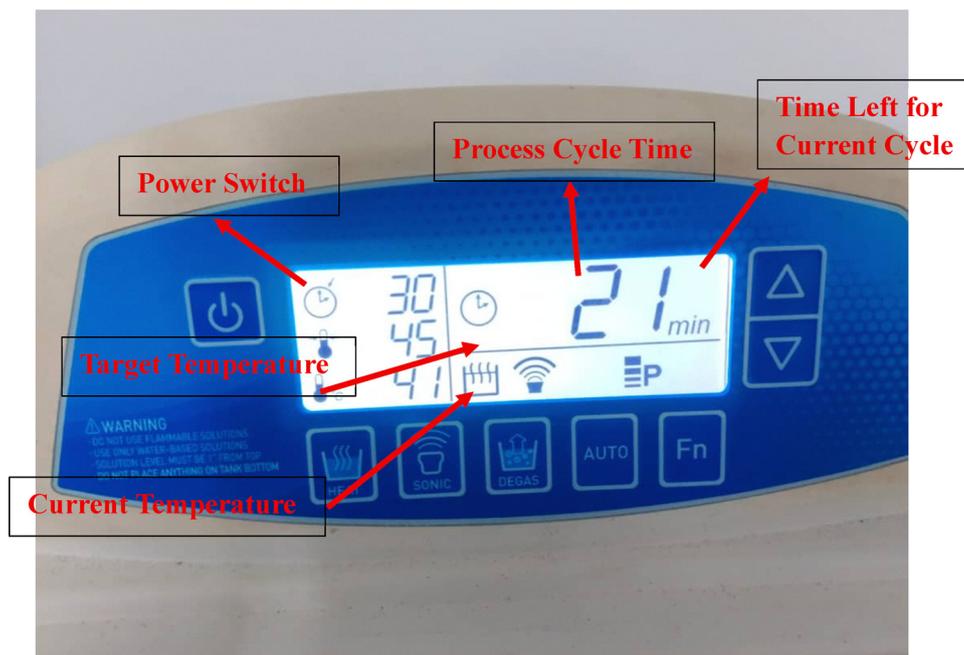
Fig. 6 Control panel settings on the Branson 3800 MH ultrasonic bath device.

before collapsing powerfully. This effective combination produces the most useful energy, particularly for processes like hydrogen production. The ANSYS simulation results support that using an ultrasonic frequency fixed at 40 kHz approaches near-optimal conditions, validating the experimental outcomes for optimisation (Fig. 7).

### 3.2 Analysis of hydrogen production rate

This section summarizes the hydrogen gas production rates during electrolysis, as shown in Table 2. The rates, measured in cubic centimetres per hour (cm³ h⁻¹), vary across different catalysts and temperatures for both electrolysis and sonoelectrolysis. For each experimental condition, measurements were repeated three times, and only minor variations were observed among the replicates. The resulting low standard deviation values confirm the good reproducibility and reliability of the experimental measurements. Results further indicate that sonoelectrocatalysis using the Branson 3800 MH ultrasonic bath achieved significantly higher production rates than electrocatalysis alone. This increase is due to ultrasonic vibrations and bubble cavitation, which enhance mass transfer and provide a consistent supply of reactants to the electrodes.

Fig. 8 presents hydrogen production rates from 17 runs for both electrocatalysis and sonoelectrocatalysis. In electrocatalysis, the highest rate occurred in Run 1 with NiO at 60 °C, producing 62 cm³ h⁻¹, while the lowest was in Run 6 with MnO₂ at 30 °C, yielding 41.6 cm³ h⁻¹. Sonoelectrocatalysis showed a similar trend, with Run 1 again leading to NiO at 60 °C, achieving 66.8 cm³ h⁻¹—while the lowest rate (44.8 cm³ h⁻¹) appeared in Runs 13 and 17, both using MnO₂ at 30 °C. Across all runs, the green line (sonoelectrocatalysis) remains above the orange line (electrocatalysis), indicating that ultrasound consistently boosts

production under all catalyst–temperature combinations. The parallel patterns of both lines suggest similar responses to experimental conditions, with sonoelectrocatalysis consistently delivering higher performance.

Among the investigated conditions, sonoelectrolysis showed the most consistent and pronounced enhancement at 45 °C, with the magnitude of improvement following the inherent catalytic activity. However, no strictly uniform trend was observed at 30 °C and 60 °C.

To illustrate the measurement uncertainty and reproducibility of the experiments, Fig. 9 presents the mean hydrogen production values for electrolysis and sonoelectrolysis, along with the corresponding standard deviations from three repeated measurements for each run.

The small magnitude of the standard deviation across all runs confirms the good reproducibility of the experimental measurements.

### 3.3 Analysis of energy efficiency

The first step in electrolysis is to determine the hydrogen's HHV, approximately 12.7 MJ Nm⁻³.[39] The value indicates the energy released from burning one normal cubic meter (Nm³) of hydrogen. To determine energy efficiency, measure the hydrogen production rate in cm³ per hour. Convert this volume to Nm³ and multiply by the hydrogen's HHV for energy output. For energy input, measure voltage and current using a power supply and multimeter, and then multiply these by the experiment's duration in hours. Finally, divide the energy output by the energy input to assess efficiency. The formula for this calculation is presented in eqn (iii).[40]

$$\text{Energy efficiency} = \frac{\text{HHV of H}_2 \times \text{H}_2 \text{ production rate}}{\text{Voltage} \times \text{Current} \times \text{Time}} \times 100\%$$

(iii)
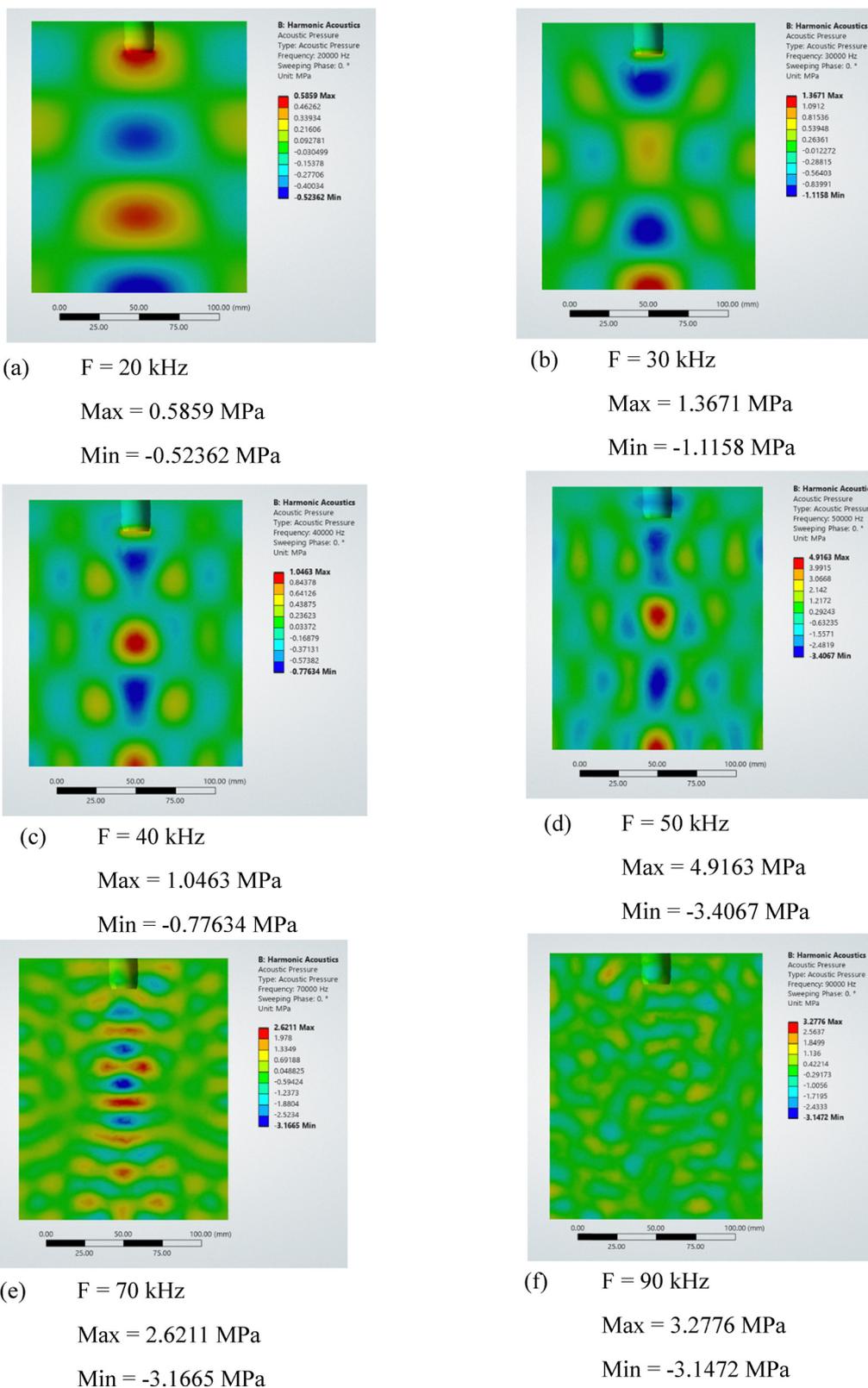
Fig. 7   Acoustic pressure distribution at different ultrasonic frequencies: (a) 20 kHz, (b) 30 kHz, (c) 40 kHz, (d) 50 kHz, (e) 70 kHz, and (f) 90 kHz.

To calculate the energy efficiency of the sonolysis process, both electrical and ultrasonic energy inputs are considered.

Electrical energy is determined by multiplying the applied voltage, current, and duration of the experiment. Ultrasonic

Table 2 Hydrogen production rate for electrocatalysis and sonoelectrocatalysis

| Run | Operating temperature (°C) | Types of catalyst | Electrocatalysis | | | | | | Sonoelectrocatalysis | | | | | |
|---|---|---|---|---|---|---|---|---|---|---|---|---|---|---|
| | | | Hydrogen production in 5 minutes ($cm^3$) | | | | | Hydrogen production ($cm^3\ h^{-1}$) | Hydrogen production in 5 minutes ($cm^3$) | | | | | Hydrogen production ($cm^3\ h^{-1}$) |
| | | | 1 | 2 | 3 | Average | Standard deviation | | 1 | 2 | 3 | Average | Standard deviation | |
| 1 | 60 | NiO | 5.2 | 5.1 | 5.2 | 5.17 | 0.058 | 62 | 5.6 | 5.5 | 5.6 | 5.57 | 0.058 | 66.8 |
| 2 | 45 | NiO | 4.6 | 4.3 | 4.5 | 4.47 | 0.153 | 53.6 | 5.2 | 5.0 | 5.1 | 5.10 | 0.1 | 61.2 |
| 3 | 45 | CoO | 4.3 | 4.6 | 4.2 | 4.37 | 0.208 | 52.4 | 5.1 | 5.0 | 4.9 | 5.00 | 0.1 | 60 |
| 4 | 45 | CoO | 4.6 | 4.4 | 4.7 | 4.57 | 0.153 | 54.8 | 5.0 | 4.8 | 5.0 | 4.93 | 0.115 | 59.2 |
| 5 | 30 | $MnO_2$ | 3.7 | 3.3 | 3.6 | 3.53 | 0.208 | 42.4 | 3.7 | 3.7 | 4.0 | 3.80 | 0.173 | 45.6 |
| 6 | 30 | $MnO_2$ | 3.6 | 3.5 | 3.3 | 3.47 | 0.153 | 41.6 | 3.9 | 3.8 | 3.6 | 3.77 | 0.153 | 45.2 |
| 7 | 60 | CoO | 5.0 | 4.8 | 5.1 | 4.97 | 0.153 | 59.6 | 5.3 | 5.6 | 5.4 | 5.43 | 0.153 | 65.2 |
| 8 | 30 | NiO | 3.9 | 4.0 | 3.9 | 3.93 | 0.058 | 47.2 | 4.4 | 4.2 | 4.5 | 4.37 | 0.153 | 52.4 |
| 9 | 45 | $MnO_2$ | 4.0 | 4.1 | 3.8 | 3.97 | 0.153 | 47.6 | 4.5 | 4.6 | 4.3 | 4.47 | 0.153 | 53.6 |
| 10 | 30 | NiO | 4.0 | 4.2 | 3.9 | 4.03 | 0.153 | 48.4 | 4.2 | 4.3 | 4.3 | 4.27 | 0.058 | 51.2 |
| 11 | 30 | CoO | 3.8 | 3.8 | 3.6 | 3.73 | 0.115 | 44.8 | 3.9 | 4.2 | 4.1 | 4.07 | 0.153 | 48.8 |
| 12 | 45 | $MnO_2$ | 4.3 | 4.1 | 4.0 | 4.13 | 0.153 | 49.6 | 4.6 | 4.3 | 4.4 | 4.43 | 0.153 | 53.2 |
| 13 | 30 | $MnO_2$ | 3.7 | 3.5 | 3.6 | 3.60 | 0.1 | 43.2 | 3.7 | 3.6 | 3.9 | 3.73 | 0.153 | 44.8 |
| 14 | 60 | CoO | 4.8 | 4.9 | 5.1 | 4.93 | 0.153 | 59.2 | 5.4 | 5.6 | 5.5 | 5.50 | 0.1 | 66 |
| 15 | 45 | NiO | 4.3 | 4.6 | 4.6 | 4.50 | 0.173 | 54 | 5.1 | 5.3 | 5.2 | 5.20 | 0.1 | 62.4 |
| 16 | 60 | $MnO_2$ | 4.7 | 4.2 | 4.8 | 4.57 | 0.321 | 54.8 | 4.8 | 4.7 | 5.0 | 4.83 | 0.153 | 58 |
| 17 | 30 | $MnO_2$ | 3.5 | 3.6 | 3.8 | 3.63 | 0.153 | 43.6 | 3.9 | 3.6 | 3.7 | 3.73 | 0.153 | 44.8 |
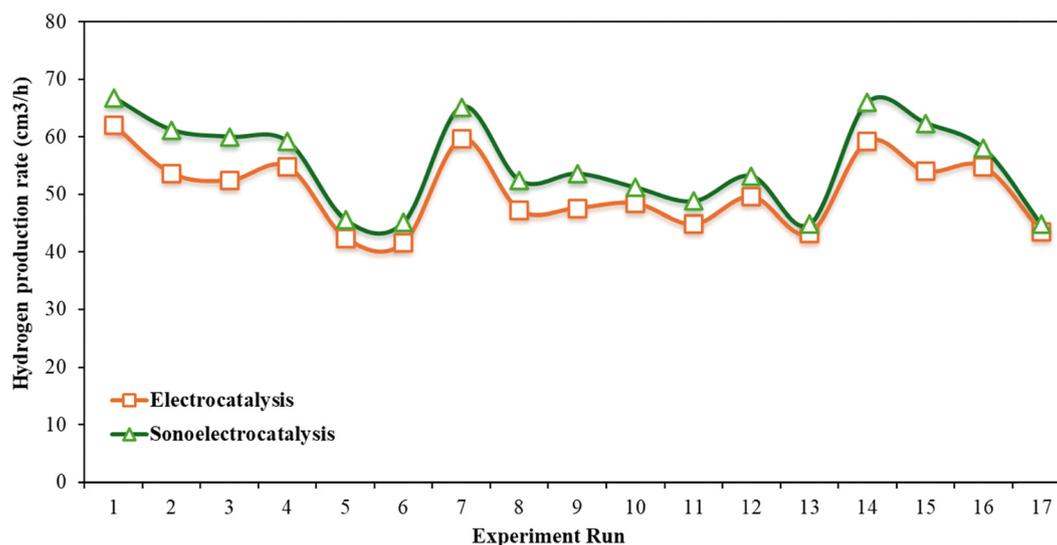


Fig. 8 Hydrogen production rate of electrocatalysis and sonoelectrocatalysis for each experiment run.

energy is calculated from the input power of the ultrasonic source, adjusted for acoustic conversion efficiency, which is evaluated using the calorimetric method by measuring the temperature rise in the liquid. During the experiment, the temperature increase of the electrolyte was recorded with a thermometer, and the acoustic power delivered was calculated using eqn (iv).[41]

$$\text{Acoustic power} = m \times Cp \times \frac{\Delta T}{t} \qquad \text{(iv)}$$

For 10 minutes, 200 ml (0.2 kg) of water experienced a temperature rise of 3.0 °C. Using the specific heat capacity of water (4184 J $kg^{-1}$ $K^{-1}$), the acoustic power calculated through eqn (iv) is 41.84 W.

$$\text{Acoustic power} = 0.2 \times 4184 \times \frac{3.0}{10 \times 60} = 4.184\ \text{W}$$

The acoustic conversion efficiency (ACE) is determined by comparing the known acoustic power to the electrical input power of the ultrasound device, as shown in eqn (v)[42]

$$\text{ACE (\%)} = \frac{\text{Acoustic power output}}{\text{Electrical power input}} \times 100\% \qquad \text{(v)}$$

The electrical power input of the Branson 3800 MH ultrasonic bath is 110 W. Since its working efficiency is 70% in low power mode, the ACE in this case is as presented through the
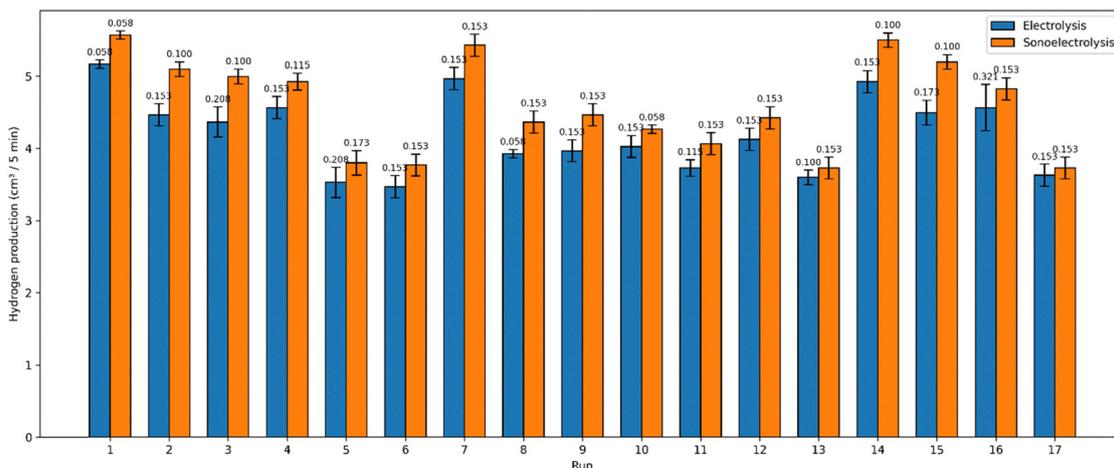
**Fig. 9** Hydrogen production for electrolysis and sonoelectrolysis ($cm^3$/5 min) with standard deviation error bars.

calculation below.

$$ACE\ (\%) = \frac{4.184}{0.7 \times 110} \times 100\% = 5.434\%$$

This percentage represents how much of the supplied electrical energy is actually converted into acoustic energy that contributes to cavitation and mixing in the solution. A high acoustic conversion efficiency indicates that the ultrasonic system is effectively transmitting energy into the medium. After that, by multiplying this value by the 110 W of input ultrasound power, the effective ultrasonic power is calculated to be 5.977 W.

The total energy input is the sum of the electrical energy and the effective ultrasonic energy, where both are measured over the same time period. Finally, the energy efficiency is obtained by dividing the energy output by the total energy input, where the result is expressed as a percentage. The full formula used

for this calculation is shown in eqn (vi).[43]

$$\text{Energy efficiency} = \frac{12.7 \times R_{cm^3/hour}}{3600 \times (V \times I + 5.977)} \times 100\% \quad \text{(vi)}$$

The energy efficiency results for all 17 experimental runs of the electrolysis process are organized and tabulated in Table 3. These results help to evaluate how effectively electrical energy was converted into hydrogen production under different conditions. The results demonstrate that the sonoelectrocatalysis process significantly enhances hydrogen production compared to standard electrocatalysis. Across most of the 17 experimental runs, the hydrogen production rate in sonoelectrolysis was consistently higher. For example, Run 1 with NiO at 60 °C produced 66.8 $cm^3$ $h^{-1}$ of hydrogen, while Run 2 and Run 3 also recorded high values of 61.2 $cm^3$ $h^{-1}$ and 59.0 $cm^3$ $h^{-1}$, respectively. These figures highlight the positive impact of ultrasonic waves in boosting the electrochemical reaction.

**Table 3** Energy efficiency for electrocatalysis and sonoelectrocatalysis

| Run | Operating temperature (°C) | Types of catalyst | Electrocatalysis | | | Sonoelectrocatalysis | | |
|-----|---------------------------|-------------------|-------------------|-------------|-------------------|----------------------|-------------|-------------------|
| | | | Hydrogen production ($cm^3$ $h^{-1}$) | Current (A) | Energy efficiency (%) | Hydrogen production ($cm^3$ $h^{-1}$) | Current (A) | Energy efficiency (%) |
| 1 | 60 | NiO | 62 | 0.50 | 4.37 | 66.8 | 0.52 | 2.11 |
| 2 | 45 | NiO | 53.6 | 0.48 | 3.94 | 61.2 | 0.50 | 1.97 |
| 3 | 45 | CoO | 52.4 | 0.45 | 4.11 | 60 | 0.46 | 2.00 |
| 4 | 45 | CoO | 54.8 | 0.46 | 4.20 | 59.2 | 0.48 | 1.94 |
| 5 | 30 | $MnO_2$ | 42.4 | 0.42 | 3.56 | 45.6 | 0.45 | 1.54 |
| 6 | 30 | $MnO_2$ | 41.6 | 0.41 | 3.58 | 45.2 | 0.41 | 1.58 |
| 7 | 60 | CoO | 59.6 | 0.49 | 4.29 | 65.2 | 0.50 | 2.10 |
| 8 | 30 | NiO | 47.2 | 0.45 | 3.70 | 52.4 | 0.46 | 1.75 |
| 9 | 45 | $MnO_2$ | 47.6 | 0.43 | 3.91 | 53.6 | 0.45 | 1.80 |
| 10 | 30 | NiO | 48.4 | 0.47 | 3.63 | 51.2 | 0.48 | 1.68 |
| 11 | 30 | CoO | 44.8 | 0.43 | 3.68 | 48.8 | 0.44 | 1.66 |
| 12 | 45 | $MnO_2$ | 49.6 | 0.44 | 3.98 | 53.2 | 0.47 | 1.76 |
| 13 | 30 | $MnO_2$ | 43.2 | 0.40 | 3.81 | 44.8 | 0.43 | 1.54 |
| 14 | 60 | CoO | 59.2 | 0.48 | 4.35 | 66 | 0.49 | 2.14 |
| 15 | 45 | NiO | 54 | 0.47 | 4.05 | 62.4 | 0.50 | 2.01 |
| 16 | 60 | $MnO_2$ | 54.8 | 0.46 | 4.20 | 58 | 0.47 | 1.92 |
| 17 | 30 | $MnO_2$ | 43.6 | 0.42 | 3.66 | 44.8 | 0.43 | 1.54 |

However, when considering energy efficiency, the results from sonoelectrocatalysis are less consistent and generally lower than those observed in electrocatalysis. In the same runs mentioned above, the energy efficiencies in sonoelectrocatalysis were 2.11%, 1.97%, and 2.00%, respectively, whereas in electrocatalysis they were noticeably higher at 4.37%, 3.94%, and 3.62%. This indicates that although ultrasound increases the hydrogen output, it also introduces additional energy consumption that lowers the overall efficiency of the process. The energy used by the ultrasonic system may not directly contribute to hydrogen generation and can lead to thermal and mechanical losses.

This lower energy efficiency is mainly due to the system configuration used in the present study. The ultrasonic energy was supplied through a commercial ultrasonic bath, in which only a portion of the input power is effectively transferred to the electrolyte, while the remaining energy is dissipated in the surrounding bath medium and reactor walls. As a result, part of the ultrasonic energy does not directly contribute to hydrogen generation. Similarly, the relatively low energy efficiency observed in conventional electrolysis is associated with the use of a small-scale laboratory setup employing non-optimized carbon electrodes and the absence of heat recovery or system-level optimization. It should be noted that the purpose of this study is not to demonstrate industrial-scale efficiency, but to compare electrolysis and sonoelectrolysis under identical laboratory conditions and to elucidate the performance trends and trade-offs introduced by ultrasound assistance.

The graph in Fig. 9 clearly illustrates that standard electrocatalysis is obviously more energy-efficient than sonoelectrocatalysis under all tested conditions. The reason for this large and consistent gap is the high energy demand of the ultrasound process itself. Energy efficiency refers to the ratio of useful energy output to the total energy input. While sonication can increase the rate of hydrogen production, it requires a significant amount of additional electrical energy to power the ultrasonic equipment. This large energy input drastically lowers

the overall efficiency calculation, even though more hydrogen is produced. In summary, sonoelectrocatalysis offers a clear advantage in terms of increasing hydrogen production, particularly when using catalysts like NiO or CoO at higher operating temperatures. However, this improvement comes at the cost of reduced energy efficiency compared to conventional electrocatalysis (Fig. 10).

### 3.4 Regression model and analysis of variance (ANOVA)

The ANOVA analysis for $H_2$ production rate and energy efficiency during electrolysis reveals that the two-factor interaction (2FI) model is highly significant, indicated by high $F$-values and a $p$-value less than 0.0001, suggesting only a 0.01% chance that the results are due to random noise. Both operating temperature (Factor A) and Types of catalyst (Factor B) significantly impact hydrogen production, with $p$-values $< 0.0001$. However, Factor B does not significantly affect energy efficiency, and the AB interaction is not significant ($p$-values 0.3904 and 0.5945), indicating independence between factors.

For sonoelectrolysis, the ANOVA model is extremely significant ($F$-values of 554.57 and 136.50, $p < 0.0001$). Both factors also show high significance, but sonoelectrolysis involves more complexity, requiring a Quadratic model compared to the simpler linear model for standard electrolysis. This suggests that ultrasound introduces complex, non-linear responses to temperature changes, as evidenced by the significance of $A^2$ in sonoelectrolysis *versus* linear effects in electrolysis (Table 4).

The model's quality is further supported by fit statistics, as shown in Table 5. The $R$-squared ($R^2$) value of more than 0.9 indicates that the model can explain 90% and above of the variation in the hydrogen production and energy efficiency data. Furthermore, the adjusted $R^2$ and predicted $R^2$ are in reasonable agreement with differences less than 0.2 for each category, suggesting the model has excellent predictive capability and is not overfitted. The high value of adequate precision is excellent for measuring the signal-to-noise ratio. Since it is well above the desired minimum of 4, it confirms that the
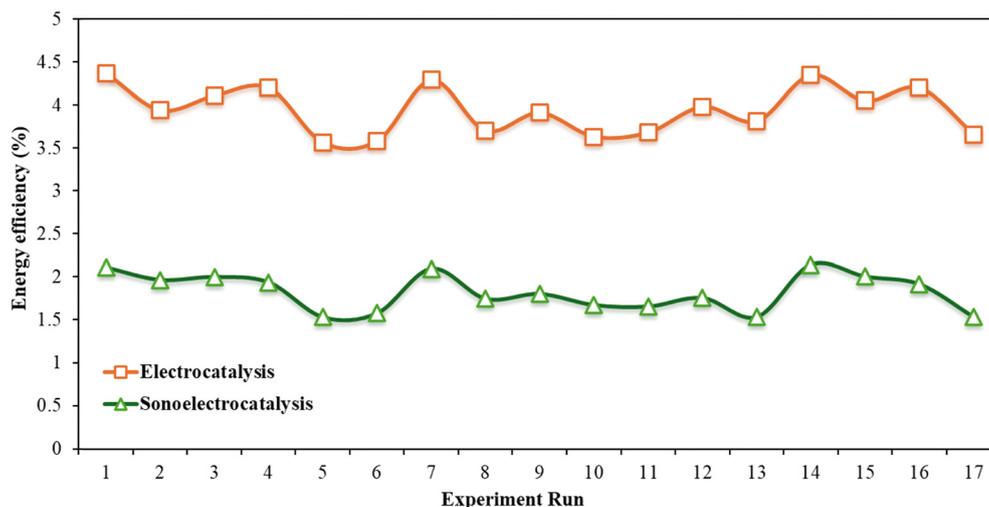


**Fig. 10** Energy efficiency of electrocatalysis and sonoelectrocatalysis for each run.

**Table 4** $p$-Values of various sources in ANOVA

| Source | $p$-Value for electrocatalysis process | | $p$-Value for sonoelectrocatalysis process | |
| --- | --- | --- | --- | --- |
| | Hydrogen production rate | Energy efficiency | Hydrogen production rate | Energy efficiency |
| Model | 2FI | 2FI | Quadratic | Quadratic |
| $F$-value ($p$-value) | 117.04 ($<$0.0001) | 30.42 ($<$0.0001) | 554.57 ($<$0.0001) | 136.50 ($<$0.0001) |
| A | $<$0.0001 | $<$0.0001 | $<$0.0001 | $<$0.0001 |
| B | $<$0.0001 | 0.1325 | $<$0.0001 | $<$0.0001 |
| $A^2$ | — | — | $<$0.0001 | 0.0017 |
| AB | 0.3904 | 0.5945 | 0.0030 | 0.1872 |
| Coefficient of variation | 2.08 | 2.22 | 0.9745 | 1.62 |
| Lack of fit | 0.3373 | 0.3203 | 0.6517 | 0.6434 |

**Table 5** Fit statistics in ANOVA

| Source | Electrocatalysis | | Sonoelectrocatalysis | |
| --- | --- | --- | --- | --- |
| | Hydrogen production rate | Energy efficiency | Hydrogen production rate | Energy efficiency |
| $R^2$ | 0.9815 | 0.9326 | 0.9970 | 0.9879 |
| Adjusted $R^2$ | 0.9732 | 0.9019 | 0.9952 | 0.9807 |
| Predicted $R^2$ | 0.9487 | 0.8098 | 0.9904 | 0.9610 |
| Adeq precision | 30.0007 | 13.6596 | 63.4690 | 30.3781 |

**Table 6** Validation of the optimised results in electrocatalysis

| | $H_2$ production rate ($cm^3$ $h^{-1}$) | Energy efficiency (%) |
| --- | --- | --- |
| Model response | 61.37 | 4.36 |
| Experimental | 62 | 4.37 |
| Error (%) | 1.02 | 0.23 |

model can be effectively used to navigate the design space and make predictions.

### 3.5 Numerical optimisation results

The numerical optimisation feature in Design-Expert effectively identifies the ideal combination of experimental factors to maximise hydrogen production rate and energy efficiency. This study aims to determine the optimal operating temperature and catalyst type. Predicted results for both metrics are presented in Table 6, showing a small error margin of 0.23% to 1.02% when compared to actual experimental results. This close match indicates that the optimisation approach is effective in enhancing electrocatalysis performance, confirming the model's success in improving $H_2$ production and energy efficiency.

In sonoelectrocatalysis, the results in Table 7 indicate a low error, with deviations of 0.37% for hydrogen production and 0.93% for energy efficiency. These values confirm that the optimized conditions are accurate and effective. The minimal differences between predicted and actual results suggest that the use of NiO

**Table 7** Validation of the optimized results in sonoelectrocatalysis

| | $H_2$ production rate ($cm^3$ $h^{-1}$) | Energy efficiency (%) |
| --- | --- | --- |
| Model response | 66.95 | 2.12 |
| Experimental | 67.2 | 2.14 |
| Error (%) | 0.37 | 0.93 |

at its optimal temperature is reliable for achieving efficient performance in sonoelectrocatalytic applications.

## 4. Conclusion

This research optimized hydrogen production through standard electrolysis and ultrasound-assisted sonoelectrolysis, evaluating the catalytic performance of NiO, CoO, and $MnO_2$ at various temperatures. Sonoelectrolysis achieved a higher production rate of 67.2 $cm^3$ $h^{-1}$ compared to 62 $cm^3$ $h^{-1}$ for standard electrolysis but had lower energy efficiency, peaking at 2.14% *versus* 4.37% for standard electrolysis. Both processes were most effective at a high temperature of 60 °C using the NiO catalyst.

The study revealed that ultrasound significantly impacts process dynamics, leading to more complex interactions, while standard electrolysis showed more linear relationships among factors. Regression models for sonoelectrolysis demonstrated reliability with low error rates, providing insights into its advantages and limitations for future green hydrogen applications.

### 4.1 Future scope and industrial scalability

A primary focus for future work should be improving the energy efficiency and Faraday efficiency of the sonoelectrolysis process. Future investigations could explore the effects of using pulsed ultrasound instead of continuous sonication, as this may reduce overall energy consumption while still benefiting from acoustic cavitation. Additionally, further studies on the impact of different ultrasonic frequencies and power levels are recommended, as initial simulations indicated that these are crucial factors that can be optimized to achieve a better balance between production rate and energy input. In addition, evaluating morphological changes and long-term catalyst stability using post-reaction SEM analysis under ultrasound conditions is necessary.

An important area for future research is the investigation of advanced catalyst materials. While this study identified NiO as the most effective among the three tested catalysts, future work could examine a wider range of materials specifically designed for the high-energy sonoelectrochemical environment.

Lastly, a comprehensive techno-economic analysis is recommended to evaluate the real-world viability of sonoelectrocatalysis. This analysis should weigh the costs of catalysts and high

energy consumption against the increased hydrogen yield to determine its potential role in future green energy systems.

## Nomenclature

| DOE | Design of experiments |
| --- | --- |
| RSM | Response surface methodology |
| GHG | Greenhouse gas |
| OER | Oxygen evolution reaction |
| HER | Hydrogen evolution reaction |
| HHV | Higher heating value |
| NiO | Nickel(II) oxide |
| CoO | Cobalt(II) oxide |
| $MnO_2$ | Manganese(IV) oxide |
| $H_2$ | Hydrogen |

## Conflicts of interest

There are no conflicts to declare.

## Data availability

All data supporting the findings of this study, including hydrogen production rates, energy efficiency measurements, regression analyses, and CFD simulation results, are fully available within the article. No additional datasets were generated or analysed beyond those reported in this manuscript.

## Acknowledgements

## References

1 A. Pan, S. Xu and S. A. H. Zaidi, Environmental impact of energy imports: Natural resources income and natural gas production profitability in the Asia-Pacific Economic Cooperation Countries, *Geosci. Front.*, 2024, **15**(2), 101756, DOI: 10.1016/j.gsf.2023.101756.

2 R.-T. Gao, *et al.*, Photoelectrochemical production of disinfectants from seawater, *Nat. Sustainability*, 2025, **8**(6), 672–681, DOI: 10.1038/s41893-025-01530-y.

3 "CO2 Emissions – Global Energy Review 2025 – Analysis - IEA." Accessed: Aug. 13, 2025. [Online]. Available: https://www.iea.org/reports/global-energy-review-2025/co2-emissions.

4 K. Attanayake, *et al.*, Renewable energy as a solution to climate change: Insights from a comprehensive study across nations, *PLoS One*, 2024, **19**(6), e0299807, DOI: 10.1371/journal.pone.0299807.

5 T. J. Wallington, M. Woody, G. M. Lewis, G. A. Keoleian, E. J. Adler, J. R. R. A. Martins and M. D. Collette, Green hydrogen pathways, energy efficiencies, and intensities for ground, air, and marine transportation, *Joule*, 2024, **8**, 2190–2207, DOI: 10.1016/j.joule.2024.07.012.

6 M. M. Hossain Bhuiyan and Z. Siddique, Hydrogen as an alternative fuel: A comprehensive review of challenges and opportunities in production, storage, and transportation, *Int. J. Hydrogen Energy*, 2025, **102**, 1026–1044, DOI: 10.1016/j.ijhydene.2025.01.033.

7 K. Su, S. Ren, R. Gao, G. Bai, L. Wu and L. Wang, Bias-Free Solar-Driven Ammonia Coupled to C 3 -Dihydroxyacetone Production through Photoelectrochemistry, *Angew. Chem., Int. Ed.*, 2025, **64**(14), DOI: 10.1002/anie.202422443.

8 C. W. Ong, J.-X. Lin, M.-L. Tsai, K. S. Thoe and C.-L. Chen, Techno-economic and carbon emission analyses of a methanol-based international renewable energy supply chain, *Int. J. Hydrogen Energy*, 2024, **49**, 1572–1585, DOI: 10.1016/j.ijhydene.2023.10.191.

9 J. Yu, R. Gao, X. Guo, N. Truong Nguyen, L. Wu and L. Wang, Electrochemical Nitrate Reduction to Ammonia on AuCu Single-Atom Alloy Aerogels under Wide Potential Window, *Angew. Chem., Int. Ed.*, 2025, **64**(4), DOI: 10.1002/anie.202415975.

10 S. Shiva Kumar and V. Himabindu, Hydrogen production by PEM water electrolysis – A review, *Mater. Sci. Energy Technol.*, 2019, **2**(3), 442–454, DOI: 10.1016/j.mset.2019.03.002.

11 H. Kouchaki-Penchah, *et al.*, The role of hydrogen in a net-zero emission economy under alternative policy scenarios, *Int. J. Hydrogen Energy*, 2024, **49**, 173–187, DOI: 10.1016/j.ijhydene.2023.07.196.

12 X. Li, Z. Wang and L. Wang, Metal–Organic Framework-Based Materials for Solar Water Splitting, *Small Sci.*, 2021, **1**, 2000074, DOI: 10.1002/smsc.202000074.

13 M. Sharifishourabi, I. Dincer and A. Mohany, Implementation of experimental techniques in ultrasound-driven hydrogen production: A comprehensive review, *Int. J. Hydrogen Energy*, 2024, **62**, 1183–1204, DOI: 10.1016/j.ijhydene.2024.03.013.

14 N. Merabet and K. Kerboua, Sonolytic and ultrasound-assisted techniques for hydrogen production: A review based on the role of ultrasound, *Int. J. Hydrogen Energy*, 2022, **47**, 17879–17893, DOI: 10.1016/j.ijhydene.2022.04.108.

15 S. Merouani, O. Hamdaoui, Y. Rezgui and M. Guemini, Theoretical estimation of the temperature and pressure within collapsing acoustical bubbles, *Ultrason. Sonochem.*, 2014, **21**(1), 55–59, DOI: 10.1016/j.ultsonch.2013.05.008.

16 F. Foroughi, C. Immanuel Bernäcker, L. Röntzsch and B. G. Pollet, Understanding the Effects of Ultrasound (408 kHz) on the Hydrogen Evolution Reaction (HER) and the Oxygen Evolution Reaction (OER) on Raney-Ni in Alkaline Media, *Ultrason. Sonochem.*, 2022, **84**, 105979, DOI: 10.1016/j.ultsonch.2022.105979.

17 S. S. Rashwan, I. Dincer, A. Mohany and B. G. Pollet, The Sono-Hydro-Gen process (Ultrasound induced hydrogen production): Challenges and opportunities, *Int. J. Hydrogen Energy*, 2019, **44**, 14500–14526, DOI: 10.1016/j.ijhydene.2019.04.115.

18  D. Rosa, S. Lattanzio, I. Bavasso and L. Di Palma, Investigation of the synergistic effect of hydrogen peroxide and ultrasound on the photocatalytic treatment under visible light of dyes wastewater, *Chem. Eng. Sci.*, 2023, **282**, 119290, DOI: 10.1016/j.ces.2023.119290.

19  H. Chen, R. Gao, H. Chen, Y. Yang, L. Wu and L. Wang, Ruthenium And Silver Synergetic Regulation NiFe LDH Boosting Long-Duration Industrial Seawater Electrolysis, *Adv. Funct. Mater.*, 2024, **34**(25), 2315674, DOI: 10.1002/adfm.202315674.

20  A. A. Ibrahim, H. Ahmed, A. H. Fakeeha, A. E. Abasaeed, A. S. Al-Fatesh and A. I. Osman, Iron catalysts enhanced by ultrasound for methane decomposition and hydrogen generation, *Int. J. Hydrogen Energy*, 2025, **137**, 851–860, DOI: 10.1016/j.ijhydene.2024.05.079.

21  H. Su, J. Sun, C. Wang and H. Wang, Study on the influence of ultrasound on the kinetic behaviour of hydrogen bubbles produced by proton exchange membrane electrolysis with water, *Ultrason. Sonochem.*, 2024, **108**, 106968, DOI: 10.1016/j.ultsonch.2024.106968.

22  Z. Wei, X. Bai, A. L. Maximov and W. Wu, Ultrasound-assisted preparation of PdCo bimetallic nanoparticles loaded on beta zeolite for efficient catalytic hydrogen production from dodecahydro-N-ethylcarbazole, *Ultrason. Sonochem.*, 2024, **103**, 106793, DOI: 10.1016/j.ultsonch.2024.106793.

23  J. Kim, M. Woo Youn, J. Yoon, B.-K. Kim and K. Park, One-step energy-saving hydrogen production via methanol oxidation using ultrasound-assisted electrodeposition of CoP electrocatalyst, *Int. J. Hydrogen Energy*, 2025, **165**, 150918, DOI: 10.1016/j.ijhydene.2025.150918.

24  C. C. Y. Wong, D. B. Preso, Y. Qin, P. S. Sinhmar, Z. Zong and J. Kwan, Ultrasound-driven seawater splitting catalysed by TiO2 for hydrogen production, *Int. J. Hydrogen Energy*, 2025, **111**, 723–734, DOI: 10.1016/j.ijhydene.2025.02.327.

25  S. S. Rashwan, I. Dincer and A. Mohany, An investigation of ultrasonic based hydrogen production, *Energy*, 2020, **205**, 118006, DOI: 10.1016/j.energy.2020.118006.

26  A. Raveendran, M. Chandran and R. Dhanusuraman, A comprehensive review on the electrochemical parameters and recent material development of electrochemical water splitting electrocatalysts, *RSC Adv.*, 2023, **13**(6), 3843–3876, DOI: 10.1039/D2RA07642J.

27  N.-T. Suen, S.-F. Hung, Q. Quan, N. Zhang, Y.-J. Xu and H. M. Chen, Electrocatalysis for the oxygen evolution reaction: recent development and future perspectives, *Chem. Soc. Rev.*, 2017, **46**(2), 337–365, DOI: 10.1039/C6CS00328A.

28  C. Chen, *et al.*, Engineering of Self-Supported Electrocatalysts on a Three-Dimensional Nickel Foam Platform for Efficient Water Electrolysis, *Trans. Tianjin Univ.*, 2024, **30**(2), 103–116, DOI: 10.1007/s12209-024-00389-y.

29  S. Wang, A. Lu and C. J. Zhong, Hydrogen production from water electrolysis: role of catalysts, *Nano Convergence*, 2021, **8**, 4, DOI: 10.1186/s40580-021-00254-x.

30  M. H. Abdurahman, A. Z. Abdullah and N. F. Shoparwe, A comprehensive review on sonocatalytic, photocatalytic, and sonophotocatalytic processes for the degradation of antibiotics in water: Synergistic mechanism and degradation pathway, *Chem. Eng. J.*, 2021, **413**, 127412, DOI: 10.1016/j.cej.2020.127412.

31  A. Khataee, R. Hassandoost and S. Rahim Pouran, Cerium-substituted magnetite: Fabrication, characterization and sonocatalytic activity assessment, *Ultrason. Sonochem.*, 2018, **41**, 626–640, DOI: 10.1016/j.ultsonch.2017.10.028.

32  B. G. Pollet, F. Foroughi, A. Y. Faid, D. R. Emberson and M. H. Islam, Does power ultrasound (26 kHz) affect the hydrogen evolution reaction (HER) on Pt polycrystalline electrode in a mild acidic electrolyte, *Ultrason. Sonochem.*, 2020, **69**, 105238, DOI: 10.1016/j.ultsonch.2020.105238.

33  M. Sillanpää and M. Shestakova, *Electrochemical Water Treatment Methods: Fundamentals, Methods and Full Scale Applications*, 2017.

34  A. Y. Faid, A. O. Barnett, F. Seland and S. Sunde, Ni/NiO nanosheets for alkaline hydrogen evolution reaction: In situ electrochemical-Raman study, *Electrochim. Acta*, 2020, **361**, 137040, DOI: 10.1016/j.electacta.2020.137040.

35  I. C. ten Have, *et al.*, Uncovering the reaction mechanism behind CoO as active phase for CO2 hydrogenation, *Nat. Commun.*, 2022, **13**(1), 324, DOI: 10.1038/s41467-022-27981-x.

36  M. Guo, R. Deng, C. Wang and Q. Zhang, Recent progress of advanced manganese oxide-based materials for acidic oxygen evolution reaction: Fundamentals, performance optimization, and prospects, *J. Energy Chem.*, 2023, **78**, 537–553, DOI: 10.1016/j.jechem.2022.11.054.

37  R. B. Bakhaidar, *et al.*, Response Surface Methodology (RSM) Powered Formulation Development, Optimization and Evaluation of Thiolated Based Mucoadhesive Nanocrystals for Local Delivery of Simvastatin, *Polymers*, 2022, **14**(23), 5184, DOI: 10.3390/polym14235184.

38  L. S. Mustapha and K. S. Obayomi, Parametric optimization of aloe vera coagulant for nitrate removal from textile wastewater using response surface methodology (RSM), *Results Chem.*, 2025, **14**, 102111, DOI: 10.1016/j.rechem.2025.102111.

39  National Research Council and National Academy of Engineering, *The Hydrogen Economy: Opportunities, Costs, Barriers, and R&D Needs*, The National Academies Press, Washington, DC, 2004.

40  A. M. I. Noor Azam, *et al.*, Parametric Study and Electrocatalyst of Polymer Electrolyte Membrane (PEM) Electrolysis Performance, *Polymers*, 2023, **15**(3), 560, DOI: 10.3390/polym15030560.

41  L. P. Ferraz and E. K. Silva, Unraveling the Thermal Effects of High-Intensity Ultrasound: A Practical Guide to Acoustic Power Determination and Heat Management, *ACS Omega*, 2025, **10**(20), 20277–20285, DOI: 10.1021/acsomega.4c11498.

42  S. Lin and F. Zhang, Measurement of ultrasonic power and electro-acoustic efficiency of high power transducers, *Ultrasonics*, 2000, **37**(8), 549–554, DOI: 10.1016/S0041-624X(99)00076-1.

43  Y. H. Teoh, *et al.*, Optimization of catalyst for electrolysis and sono-electrolysis process for hydrogen production, *Int. J. Hydrogen Energy*, 2025, **157**, 150508, DOI: 10.1016/j.ijhydene.2025.150508.